Talanta 82 (2010) 450–457

Contents lists available at ScienceDirect

Talanta

journal homepage: www.elsevier.com/locate/talanta

# Synthesis and characteristic of the $Fe_3O_4$@$SiO_2$@Eu(DBM)$_3$·2$H_2O$/$SiO_2$ luminomagnetic microspheres with core-shell structure

Ping Lu[a,b], Ji-Lin Zhang[a,*], Yan-Lin Liu[a], De-Hui Sun[c], Gui-Xia Liu[b], Guang-Yan Hong[a], Jia-Zuan Ni[a,d]

[a] State Key Laboratory of Rare Earth Resource Utilization, Changchun Institute of Applied Chemistry, Chinese Academy of Sciences, Changchun 130022, China
[b] School of Chemistry and Environmental Engineering, Changchun University of Science and Technology, Changchun 130022, China
[c] Changchun Institute Technology, Changchun 130012, China
[d] College of Life Science, Shenzhen University, Shenzhen 518060, China

ARTICLE INFO

*Article history:*
Received 6 January 2010
Received in revised form 22 April 2010
Accepted 25 April 2010
Available online 1 June 2010

*Keywords:*
Fluorescence
Magnetic
Microsphere
Cell imaging
Eu(III) complex
Magnetite

ABSTRACT

The core-shell structured luminomagnetic microsphere composed of a $Fe_3O_4$ magnetic core and a continuous $SiO_2$ nanoshell doped with Eu(DBM)$_3$·2$H_2O$ fluorescent molecules was fabricated by a modified Stöber method combined with a layer-by-layer assembly technique. X-ray diffraction (XRD), Fourier transform infrared spectroscopy (FTIR), field emission scanning electron microscopy (FE-SEM), transmission electron microscopy (TEM), confocal microscopy, photoluminescence (PL), and superconducting quantum interface device (SQUID) were employed to characterize the $Fe_3O_4$@$SiO_2$@Eu(DBM)$_3$·2$H_2O$/$SiO_2$ microspheres. The experimental results show that the microshpere has a typical diameter of ca. 500 nm consisting of the magnetic core with about 340 nm in diameter and silica shell doped with europium complex with an average thickness of about 80 nm. It possesses magnetism with a saturation magnetization of 25.84 emu/g and negligible coercivity and remanence at room temperature and exhibits strong red emission peak originating from electric-dipole transition $^5D_0 \rightarrow {}^7F_2$ (611 nm) of $Eu^{3+}$ ions. The luminomagnetic microspheres can be uptaken by HeLa cells and there is no adverse cell reaction. These results suggest that the luminomagnetic microspheres with magnetic resonance response and fluorescence probe property may be useful in biomedical imaging and diagnostic applications.

© 2010 Elsevier B.V. All rights reserved.

## 1. Introduction

Multifunctional materials consisting of magnetic materials and fluorescent materials as well as outer biocompatible materials have attracted particular attention because of their potential biomedical applications in bioimaging such as magnetic resonance imaging (MRI), fluorescent confocal imaging and time-resolved fluorescence imaging [1–10].

Superparamagnetic iron oxide nanoparticles can be used as contrast agents because they can accelerate the transverse ($T_2$) relaxation of water protons and exhibit dark contrast [2,3]. Optical imaging probes mainly include various organic fluorescent molecules [11–13], quantum dots (QDs) [14–17], transition/lanthanide metal ions-doped luminescent compounds [18–21]. Although the fluorescent dyes have larger molar extinction coefficients [22] and the quantum dots can exhibit good photostability and strong luminescence tunable [21], the poor photostability of the fluorescent dyes and the extreme toxicity of the quantum dots always make them suffer from some limitations in biomedical applications. But then, these limitations also lead to extensive efforts to develop less toxic luminescent materials such as lanthanide-doped fluorescent probe materials [8,23–28]. Silica shell coated on the surface of the magnetic cores is an excellent biocompatible material with good stability, easy functionalization, and low cytotoxicity [18–22]. The combination of magnetic and luminescent properties into a single micro- or nanocomposite system through $SiO_2$ matrix will allow the development of a novel multifunctional biomedical platform for multimodal imaging and simultaneous diagnosis. But to optimize the combination, there still are the following challenges in the fabrication:

(1) How to increase magnetic response signal weakened by non-magnetic materials (such as fluorescent labeling and biocompatible shell) coated on the magnetic cores and to avoid magnetic aggregation caused by a large coercivity and remanence. On one hand, as magnetic cores the small magnetic nanoparticles with poor crystallization and supermparamagnetism are not easily magnetic agglomeration, but they usually suffer from relatively weak magnetic response behaviors. For example, the multifunctional composite nanoparticles with magnetic, up-conversion fluorescence and bio-affinity properties synthesized by Lu et al. had a

* Corresponding author.
*E-mail address:* zjl@ciac.jl.cn (J.-L. Zhang).

0039-9140/$ – see front matter © 2010 Elsevier B.V. All rights reserved.
doi:10.1016/j.talanta.2010.04.052

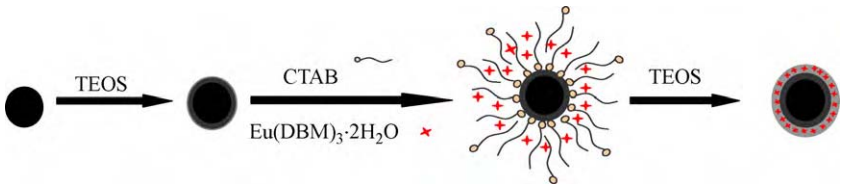


**Scheme 1.** The fabrication of the $Fe_3O_4$ @$SiO_2$@$Eu(DBM)_3{\cdot}2H_2O$/$SiO_2$ microspheres.

very low saturation magnetization values (5.3 emu/g) and relatively poor dispersibility [29]. Similarly, the core-shell structure $Fe_3O_4$@$SiO_2$-doped with Tb-complex bifunctional nanocomposites with emitting green fluorescence and magnetic behavior reported by Yu et al. only exhibited a low value (7.44 emu/g) at room temperature [30]. On the other hand, the good crystallization magnetic particulates with a large coercivity and remanence at room temperature can easily be controlled through an external magnetic field, but they easily produce magnetic agglomeration. Recently, the hydrophilic $Fe_3O_4$ microspheres (~200 nm) with high magnetic saturation magnetization (81.9 emu/g) and negligible coercivity and remanence synthesized by a solvothermal reduction method reported by Deng et al. [31] should be an ideal candidate for improvement of the magnetic response and magnetic aggregation.

(2) Fluorescent quenching of the fluorophore on the surface of the particle caused by the magnetic core, by the interaction of a number of organic dye molecules, and by solvent molecules. For instance, Ma et al. [26] reported the multifunctional magnetic-fluorescent nanocomposites with $Fe_3O_4$ nanoparticles as the core and $Eu^{3+}$-doped yttrium oxides ($Y_2O_3$:Eu) as the shell exhibited a weak fluorescence signal which might originate from the iron ion quenching effect to $Eu^{3+}$. Bertorelle et al. [32] found that the fluorescence intensity of the magnetic-fluorescent nanocomposites using fluorescein and rhodamine was 3.5 and 2 times lower than the dyes alone, respectively, and believed that the quenching process results from an energy transfer process between the fluorescent molecules and the metal oxide particles. Mandal et al. [33] also found that there was the similar behavior between iron oxide particles stabilised by oleic acid and QDs stabilised by tri-n-octylphosphine. Intermolecule quenching with a lower number of Cy5.5 molecules per particle has also been reported [34]. The rare earth complex probe materials with excellent fluorescent radiation, narrow half-peak breadth, high color purity, and large Stockes shift are easily quenched by water molecules. In addition, it is very difficult to directly attach these hydrophobic fluorescent markers onto surface of the hydrophilic magnetic particles. Zhang et al. [35] found that surfactant cetyltrimethylammonium bromide (CTAB) can make fluorescence intensity increase of the Eu-DBM-Phen (DBM: dibenzoylmethanate, Phen: 1,10-phenanthroline) complex in aqueous solution due to protection of the CTAB to fluorescent ligands, which reduced non-radiation transition originating from water molecules. Thus, the advantage should be used for improvement of the above problems.

(3) How to increase the photostability of the rare earth fluorescent probe complexes and to improve biocompatibility of the entire particles. The biocompatible silica shell coated on the surface of the magnetic cores has become a good solution by incorporating the hydrophobic rare earth fluorescent complex molecules into the $SiO_2$ shell. For example, Yuan's group has synthesized many silica-based functionalized Eu and Tb fluorescent nanoparticles for the fluoroimmunoassay and the time-resolved fluorescence imaging and actualized the sensitive homogeneous time-resolved fluoroimmunoassay and the fluorescence imaging detection of the cells [8,23,27,28].

To overcome the above problems, we describe synthesis and characteristic of a luminomagnetic bifunctional microspheres with core-shell structure (denoted as $Fe_3O_4$@$SiO_2$@$Eu(DBM)_3{\cdot}2H_2O$/$SiO_2$) in this paper, as schematically illustrated in Scheme 1. The primary goal of this research is as follows: (1) to improve the poor magnetic response and reduce magnetic conglomeration through the monodisperse submicrometer $Fe_3O_4$ particulates with negligible coercivity and remanence and a larger saturation magnetization as magnetic cores; (2) to eliminate fluorescence quenching through use of the $SiO_2$ isolation layer between $Fe_3O_4$ particulates and the europium fluorescent complex and to increase photostability through protection of the outer silica shell; (3) to enhances the fluorescent signal and increases the photostability by encapsulating the hydrophobic europium complex into hydrophilic silica shell by means of surfactant CTAB to form a fluorescent probe sandwich. The luminomagnetic microspheres with good magnetic response and fluorescence probe property as well as water-dispersibility would have potential medical applications in bioimaging.

## 2. Experimental

### 2.1. Materials

Ferric chloride ($FeCl_3{\cdot}6H_2O$), ethanol, ethylene glycol, ammonium hydroxide aqueous solution (25%) were purchased from Beijing Chemicals Corporation, China. Tetraethyl orthosilicate (TEOS), sodium acetate ($CH_3COONa$) polyethylene glycol (PEG molecular weight = 2000), cetyltrimethylammonium bromide (CTAB) were obtained from Beijing Yili Chemicals Limited Company, China. All chemicals were analytical grade and used as received without further purification. $Eu(DBM)_3{\cdot}2H_2O$ were synthesized as reported [36]. HeLa cell line was purchased from Cell Bank of Shanghai Institute of Biochemistry and Cell Biology, Chinese Academy of Sciences, China. Unless otherwise mentioned, all culture media and additives were from Hyclone, USA.

### 2.2. Synthesis

#### 2.2.1. Synthesis of $Fe_3O_4$ particles

The magnetic particles were prepared through a solvothermal reaction which was reported previously [31]. Briefly, 2.72 g of $FeCl_3{\cdot}6H_2O$ and 7.20 g of sodium acetate were dissolved in 80 mL of ethylene glycol under magnetic stirring, followed by the addition of PEG (1.00 g). The obtained homogeneous yellow solution was transferred to a Teflon-lined stainless-steel autoclave (120 mL) and sealed to heat at 180 °C. After reaction for 6 h, the autoclave was cooled to room temperature. The obtained black magnetite particles were separated using an NdFeB magnet, then washed with deionized water for four times, and finally dried in an oven at 80 °C for 12 h.

*2.2.2. Synthesis of $Fe_3O_4$@$SiO_2$ microspheres*

The core-shell $Fe_3O_4$@$SiO_2$ microspheres were prepared by a modified Stöber method [37] combined with a layer-by-layer assembly technique [38]. Briefly, 0.03 g of $Fe_3O_4$ particles (~300 nm in diameter) were treated with 0.1 M HCl aqueous solution (25 mL) by ultrasonication. After the treatment for 10 min, the magnetite particles was then separated and washed with deionized water. Subsequently, the resulting magnetite particles were homogeneously dispersed in a solution containing ethanol (160 mL), deionized water (40 mL) and concentrated ammonia aqueous solution (10.0 mL, 25 wt.%). Next, 0.4 mL of TEOS was in batches added into the above solution with ultrasonic vibrations using a syringe, namely 0.2 mL of the TEOS was injected into the reaction system every other twenty minutes till total amount of the TEOS reached 0.4 mL. After stirred at room temperature for 5 h, the $Fe_3O_4$@$SiO_2$ microspheres were separated and washed repeatedly with deionized water to remove nonmagnetic by-products. Finally, $Fe_3O_4$@$SiO_2$ microspheres were obtained.

*2.2.3. Synthesis of $Fe_3O_4$@$SiO_2$@$Eu(DBM)_3{\cdot}2H_2O$/$SiO_2$ microspheres*

The $Fe_3O_4$@$SiO_2$ spheres obtained from the above step were ultrasonically redispersed in a solution containing $Eu(DBM)_3{\cdot}2H_2O$ (8 mg), CTAB (16 mg), concentrated ammonia (0.3 mL, 25 wt.%), ethanol (60 mL) and deionized water (80 mL). Under ultrasonic processing, TEOS (0.1 mL) was injected to the solution every 20 min till the total amount of TEOS reached 0.2 mL. The mixture was magnetically stirred for 5 h. Subsequently, the suspensions were separated using an NdFeB magnet and washed with deionized water several times. Finally the obtained composite particles were dried at 80 °C.

*2.3. Cell imaging*

HeLa cells were cultured at 37 °C in a humidified atmosphere with 5% $CO_2$ in air, in 75 $cm^2$ glass culture vial containing 10 mL high-glucose DMEM medium supplemented with 10% fetal bovine serum (FBS), 1% penicillin and 1% streptomycin. The medium was changed every other day. $Fe_3O_4$@$SiO_2$@$Eu(DBM)_3{\cdot}2H_2O$/$SiO_2$ microspheres were suspended in the medium at a particle concentration of 5–10 μg/mL, after 1 h sonication in waterbath the medium containing the particles group or control group was applied to the 50–60% confluent cells. After incubated for 20 h at 37 °C, the culture vial was washed 3–5 times by phosphate-buffered saline (PBS), and then subjected to the confocal microscopy imaging detection.

*2.4. Characterizations*

The X-ray diffraction (XRD) of samples were examined on a Bruker D8FOCUS X-ray diffractometer using Cu Kα radiation (λ = 1.5406 Å) at a scanning rate of 15° $min^{-1}$ and the detective range from 10 to 80 °C. The morphology of samples was inspected on a HITACHI S-4800 field-emission scanning electron microscope (FE-SEM) and a JEOL-2010 transmission electron microscope (TEM) with an accelerating voltage of 200 kV. Fourier transform infrared (FT-IR) spectra were determined with a model FTS135 infrared spectrophotometer (American BIO-RAD Company) operated at a resolution of 2 $cm^{-1}$. Magnetic properties were detected using a superconducting quantum interface device (SQUID) magnetometer (Quantum Design MPMS XL). Photoluminescence (PL) spectra of the sample were measured by an F-4500 FL Spectrophotometer equipped with a 150-W xenon lamp as the excitation source at room temperature. Confocal microscopy images were obtained using an Olympus FluoView® FV1000 confocal microscopy with laser excitation at 405 nm.

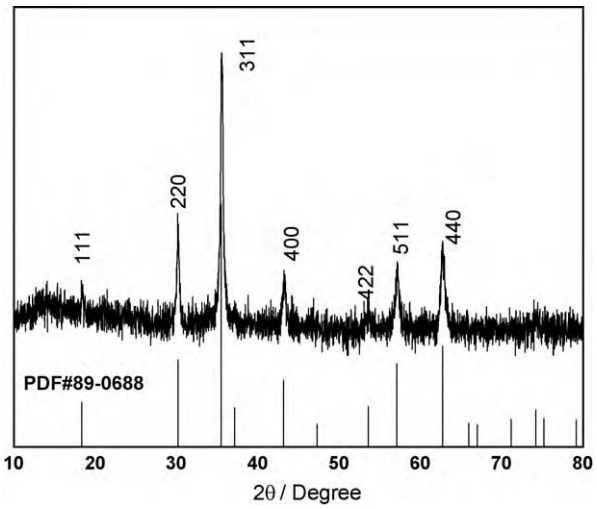


**Fig. 1.** XRD pattern of the $Fe_3O_4$ particles and $Fe_3O_4$ (JCPDS 89-0688).

## 3. Results and discussion

*3.1. Structure of the $Fe_3O_4$ microspheres*

Structure of the $Fe_3O_4$ microspheres has been examined by XRD. Fig. 1 shows the XRD profiles of the $Fe_3O_4$ particles as magnetic cores and the JCPDS 89-0688 card of $Fe_3O_4$ as the reference, respectively. As shown in Fig. 1, the position and relative intensity of all diffraction peaks match well with standard $Fe_3O_4$ powder diffraction data (JCPDS 89-0688), which indicates that the $Fe_3O_4$ particles is pure phase and belong to cubic system.

*3.2. Morphology of the $Fe_3O_4$@$SiO_2$@$Eu(DBM)_3{\cdot}2H_2O$/$SiO_2$ microspheres*

SEM images of the $Fe_3O_4$ magnetic particles, the $Fe_3O_4$@$SiO_2$ composite microspheres and the $Fe_3O_4$@$SiO_2$@$Eu(DBM)_3{\cdot}2H_2O$/$SiO_2$ luminomagnetic dual-functional microspheres are shown in Fig. 2. It can be observed from Fig. 2a and b that the $Fe_3O_4$ particulates are all uniform spherical particles with the size in the range of 330–350 nm. Surface of the $Fe_3O_4$ submicrometer particles is not smooth because they are composed of many reunited nanoparticles. Such $Fe_3O_4$ microspheres make them possess magnetism with negligible coercivity and remanence though their sizes have been over the critical magnetic size of $Fe_3O_4$ nanocrystals and be easily coated due to the relative coarse surface. SEM images of the resulting $Fe_3O_4$@$SiO_2$ composite particles are shown in Fig. 2c and d. The core-shell structural microspheres, like $Fe_3O_4$ particles, are still uniform and spherical particulates with an average diameter of ca. 490 nm and they have smoother surface than that of the uncoated $Fe_3O_4$ cores. That is to say, the smooth $Fe_3O_4$@$SiO_2$ microspheres are composed of magnetic cores with the average diameter of about 340 nm and silica shell with thickness of ca. 75 nm on average. The thickness of the silica shell can be tuned by simply varying the initial amount of TEOS. Such $Fe_3O_4$@$SiO_2$ microspheres can be well dispersed in an aqueous medium and possess good magnetic response. SEM images of the $Fe_3O_4$@$SiO_2$@$Eu(DBM)_3{\cdot}2H_2O$/$SiO_2$ microspheres are shown in Fig. 3e and f. Most of the samples still are spherical shape with an average particles size ca. 500 nm, but they have not smooth surface in comparison with the precursor of $Fe_3O_4$@$SiO_2$. This implied that the mixture of the $Eu(DBM)_3{\cdot}2H_2O$/CTAB/$SiO_2$ has deposited on the surface of the $Fe_3O_4$@$SiO_2$ microspheres. To investigate the

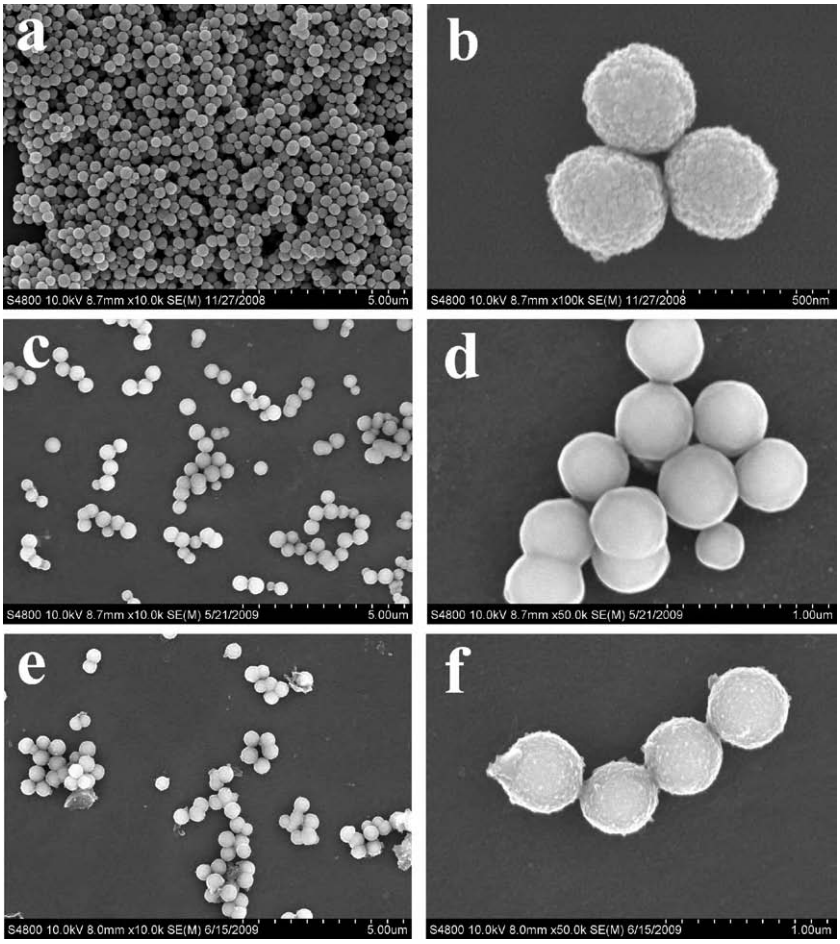


**Fig. 2.** SEM images (left: low magnification; right: high magnification) of the samples at different fabrication stage of the $Fe_3O_4$@$SiO_2$@Eu(DBM)$_3$·2$H_2O$/$SiO_2$: $Fe_3O_4$ (a, b); $Fe_3O_4$@$SiO_2$ (c, d) and $Fe_3O_4$@$SiO_2$@Eu(DBM)$_3$·2$H_2O$/$SiO_2$ (e, f).

core-shell structure in detail, the luminomagnetic dual-functional $Fe_3O_4$@$SiO_2$@Eu(DBM)$_3$·2$H_2O$/$SiO_2$ microspheres was further characterized by TEM. The TEM photographs of $Fe_3O_4$@$SiO_2$ and $Fe_3O_4$@$SiO_2$@Eu(DBM)$_3$·2$H_2O$/$SiO_2$ samples are depicted in Fig. 3. It can be clearly observed from Fig. 3 that they are composed of the black magnetic cores with about 340 nm in diameter and gray shell with an average thickness of about 75 nm for the $Fe_3O_4$@$SiO_2$ and about 80 nm for the $Fe_3O_4$@$SiO_2$@Eu(DBM)$_3$·2$H_2O$/$SiO_2$. Moreover, if carefully observed, we can find that surface of the $Fe_3O_4$@$SiO_2$ is smoother than that of the $Fe_3O_4$@$SiO_2$@Eu(DBM)$_3$·2$H_2O$/$SiO_2$ due to poor soakage of the Eu(DBM)$_3$·2$H_2O$ fluorescent complex on the surface of the $Fe_3O_4$@$SiO_2$. These results are consistent with those of SEM observation. It should be pointed that it is difficult to differentiate the inner silica layer and the outer silica layer from the TEM photographs owing to good compatibility between two silica layers.

The above electron microscope observation results can be further confirmed by FTIR spectra of the products in Fig. 4c and d. FTIR analysis shown in Fig. 4a indicates that there is a little PEG adsorbed on the surface of the $Fe_3O_4$ microspheres due to existence of characteristic absorption bands or peaks of the PEG ($\nu_{O-H}$: centered at 3437 $cm^{-1}$; $\nu_{C-H}$: 2926 and 2841 $cm^{-1}$

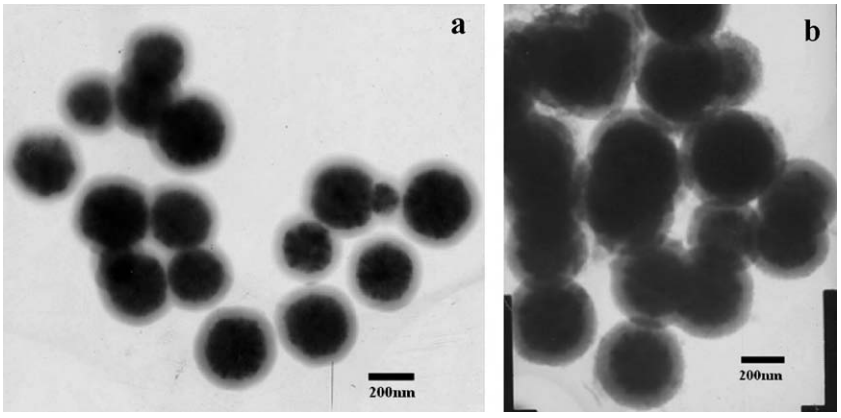


**Fig. 3.** TEM images of the $Fe_3O_4$@$SiO_2$ (a) and the $Fe_3O_4$@$SiO_2$@Eu(DBM)$_3$·2$H_2O$/$SiO_2$ (b) samples.

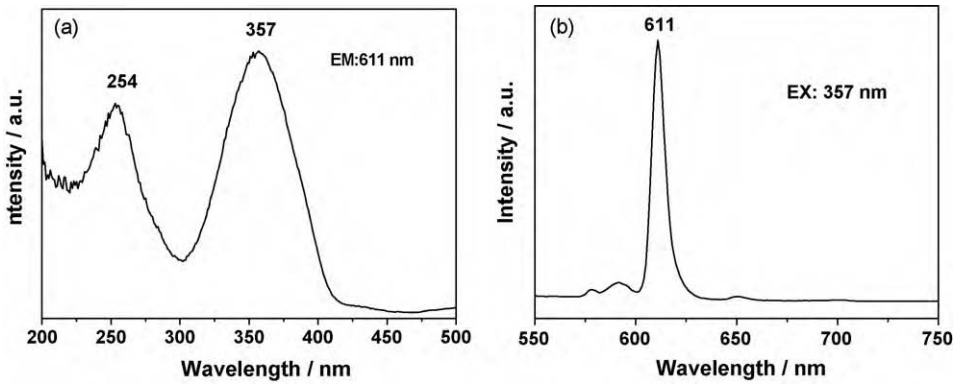


**Fig. 4.** FT-IR spectra of $Fe_3O_4$ (a), $Fe_3O_4$@$SiO_2$ (b), pure $Eu(DBM)_3{\cdot}2H_2O$ (c) and $Fe_3O_4$@$SiO_2$@$Eu(DBM)_3{\cdot}2H_2O$/$SiO_2$ (d) samples.

from $-CH_2$; $\nu_{C-O-C}$: centered at 1076 $cm^{-1}$) and the magnetite phase ($\nu_{Fe-O}$: 422, 588 and 630 $cm^{-1}$). This makes them be water-soluble and favor coating of silica in ethanol aqueous solution using the Stöber method [37]. FTIR spectra in Fig. 4b indicate that the silica shell coated on the surface of the magnetite cores can be confirmed by assignments of the bands Si—O—Si (1091, 798 $cm^{-1}$), Si—OH (945 $cm^{-1}$), and Fe—O—Si (468 $cm^{-1}$). Compared with the FT-IR spectrum of the $Fe_3O_4$@$SiO_2$ in Fig. 4b, the $Fe_3O_4$@$SiO_2$@$Eu(DBM)_3{\cdot}2H_2O$/$SiO_2$ microspheres has two sets of new characteristic FT-IR adsorption peaks to be found. One set of weak absorption peaks centered at 1479 $cm^{-1}$ ($\nu_{C-C}$: from carbon framework of the phenyl of the DBM) and 1636 $cm^{-1}$ ($\nu_{as\ C=O}$) originate from $Eu(DBM)_3{\cdot}2H_2O$, while second set of absorption peaks at 2924 and 2853 $cm^{-1}$ belong to C—H stretching vibrations rooted in $-CH_2$ and $-CH_3$ of the CTAB. Low content of the $Eu(DBM)_3{\cdot}2H_2O$ in the $Fe_3O_4$@$SiO_2$@$Eu(DBM)_3{\cdot}2H_2O$/$SiO_2$ microspheres may be responsible for its weak FT-IR absorption. Nevertheless, the aforementioned characteristic photoluminescence of the Eu (III) in the $Fe_3O_4$@$SiO_2$@$Eu(DBM)_3{\cdot}2H_2O$/$SiO_2$ microspheres can safely confirm the existence of the $Eu(DBM)_3{\cdot}2H_2O$ complex.

The results obtained from observation of SEM and TEM and analyses of the FTIR clearly demonstrate that we have achieved our main objectives in the fabrication: (1) To avoid luminescence quenching and to provide silanol groups for immobilization of the europium (III) complexes inlaid in the surfactant CTAB, a layer of silica was first coated on the surface of the $Fe_3O_4$ microspheres so as to avoid the direct contact of the $Eu(DBM)_3{\cdot}2H_2O$ with the magnetic core. (2) To incorporate $Eu(DBM)_3{\cdot}2H_2O$ into $SiO_2$ shell and deposit onto the surface of the $Fe_3O_4$@$SiO_2$ microspheres, surfactant CTAB enabling to carry the $Eu(DBM)_3{\cdot}2H_2O$ with it was used in the course of hydrolysis and condensation reactions of TEOS. CTAB plays two roles: (a) dissolving poor water-soluble $Eu(DBM)_3{\cdot}2H_2O$ into the hydrolyzing medium of TEOS; (b) carrying the $Eu(DBM)_3{\cdot}2H_2O$ with it to assembly onto the surface of the $Fe_3O_4$@$SiO_2$ microspheres utilizing sorption of the hydrophilic head of the CTAB to the silanol groups on the surface of the $Fe_3O_4$@$SiO_2$ microspheres. As a result, $Eu(DBM)_3{\cdot}2H_2O$ complex is homogeneously incorporated into the outer silica shell, which makes $Eu(DBM)_3{\cdot}2H_2O$ complex increase its thermal- and photostability.

### 3.3. *Magnetic properties of the $Fe_3O_4$@$SiO_2$@$Eu(DBM)_3{\cdot}2H_2O$/$SiO_2$ microspheres*

Fig. 5 presented the magnetic hysteresis loops of the uncoated $Fe_3O_4$ powder (a), $Fe_3O_4$@$SiO_2$ powder (b) and $Fe_3O_4$@$SiO_2$@$Eu(DBM)_3{\cdot}2H_2O$/$SiO_2$ powder (c) in an applied field

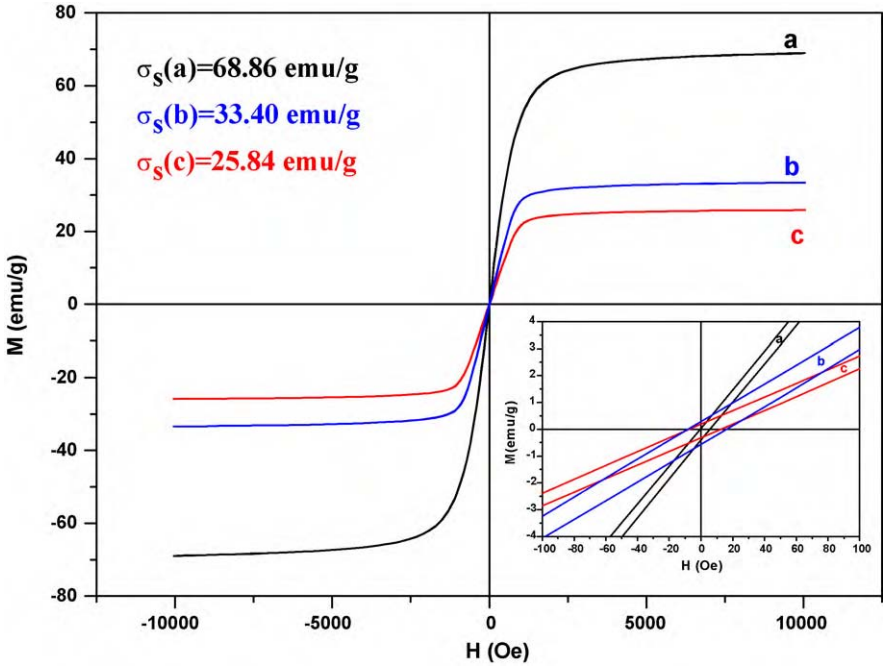


**Fig. 5.** Measured magnetic hysteresis loops of the fabricated $Fe_3O_4$ powder (a), magnetic silica beads (b) and $Fe_3O_4$@$SiO_2$@$Eu(DBM)_3{\cdot}2H_2O$/$SiO_2$ (c).

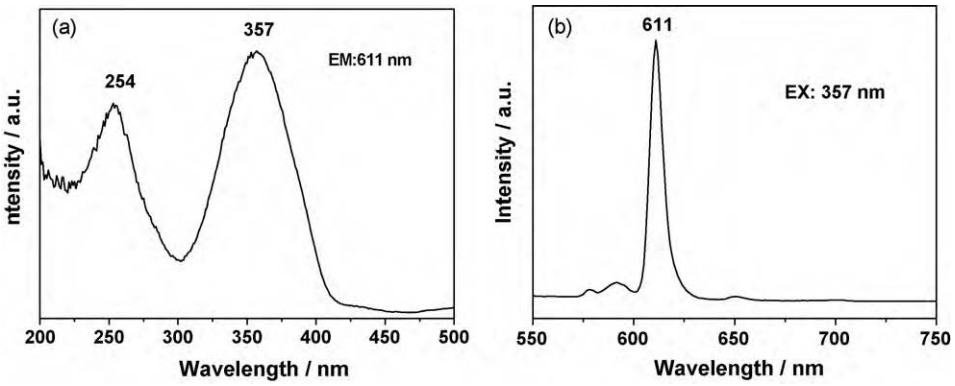


**Fig. 6.** Excitation spectrum (a) and emission spectrum (b) of $Fe_3O_4$@$SiO_2$@ Eu(DBM)$_3$·2$H_2O$/$SiO_2$ microspheres.

of 10 kOe at 300 K. It is clearly seen from these magnetic hysteresis loops that all the samples have stronger magnetism with negligible coercivity and remanence at room temperature. Their saturation magnetization was 68.86, 33.40 and 25.84 emu/g, respectively. Compared with the uncoated $Fe_3O_4$ particles, the saturation magnetization of the $Fe_3O_4$@$SiO_2$ microspheres obviously decreased because the diamagnetic contribution of the thick silica shell resulted in a low mass fraction of the $Fe_3O_4$ magnetic substance. Nevertheless, there was only smaller difference of saturation magnetization between $Fe_3O_4$@$SiO_2$ and $Fe_3O_4$@$SiO_2$@Eu(DBM)$_3$·2$H_2O$/$SiO_2$. This is because thin outermost layer Eu(DBM)$_3$·2$H_2O$/$SiO_2$ shell cannot cause a larger mass fraction change of the $Fe_3O_4$ magnetic substance from $Fe_3O_4$@$SiO_2$ to $Fe_3O_4$@$SiO_2$@Eu(DBM)$_3$·2$H_2O$/$SiO_2$. Though the saturation magnetization of $Fe_3O_4$@$SiO_2$@Eu(DBM)$_3$·2$H_2O$/$SiO_2$ particles is less than the magnetite nanoparticles as magnetic core, it may be believed to possess enough strong magnetic attraction for effectively magnetic separation.

### 3.4. Fluorescent properties of the $Fe_3O_4$@$SiO_2$@Eu(DBM)$_3$·2$H_2O$/$SiO_2$

The excitation and emission spectra of the $Fe_3O_4$@$SiO_2$@Eu(DBM)$_3$·2$H_2O$/$SiO_2$ microspheres are shown in Fig. 6a and b, respectively. The excitation spectrum was monitored at 612 nm, while the emission spectrum was measured with 357 nm as the excitation wavelength. It can be seen from the excitation spectrum in Fig. 6a that there are two broad excitation peaks at 254 and 357 nm which are due to light absorption by the diketonate ligands. Similarly, the narrow emission peaks observed in the emission spectrum (Fig. 6b) originate from transition of the $^5D_0$ excited state level to the $^7F_J$ ($J$ = 0–6) levels. The strongest emission peak at 612 nm is due to the hypersensitive electric-dipole transition of $^5D_0$–$^7F_2$. The fine structure reveals that the europium ion does not occupy a site with inversion symmetry. The spectrum testing results further prove the aforementioned conclusion that fluorescent Eu(DBM)$_3$·2$H_2O$ complex has be incorporated into the silica shell of the $Fe_3O_4$@$SiO_2$@Eu(DBM)$_3$·2$H_2O$/$SiO_2$ microspheres.

### 3.5. Dispersity and magnetic response of the $Fe_3O_4$@$SiO_2$@Eu(DBM)$_3$·2$H_2O$/$SiO_2$ microspheres in an aqueous solution

To illustrate dispersibility in aqueous medium and magnetic response to the external magnetic field, a simple experiment was performed. An optical photograph of the magnetic microspheres attracted by an external magnet is exhibited in Fig. 7. When a magnet was placed close to the glass vial holding the magnetic microsheres dispersed in deionized water, the microsheres were attracted towards the magnet very quickly and accumulated to the side of the glass vial near the magnet within two minutes, and

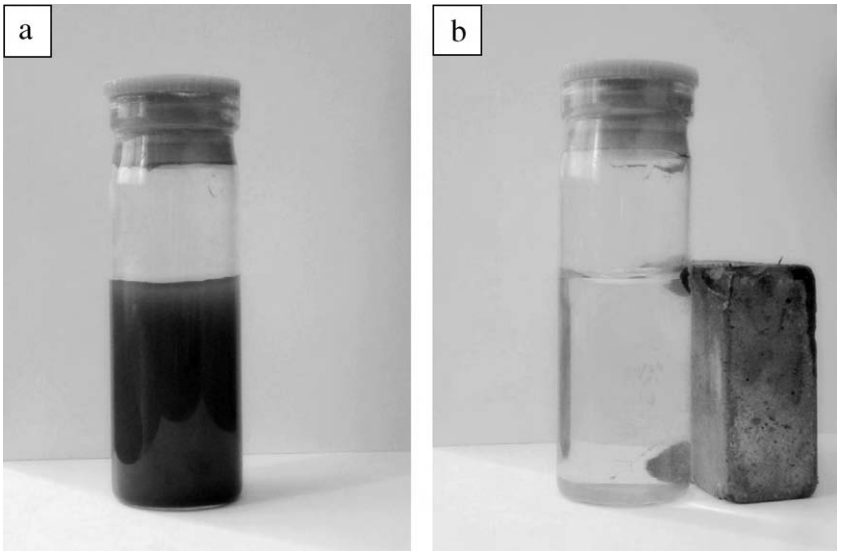


**Fig. 7.** Photographs of aqueous solutions of the $Fe_3O_4$@$SiO_2$@Eu(DBM)$_3$·2$H_2O$/$SiO_2$ microspheres without (a) and with (b) magnetic field applied.

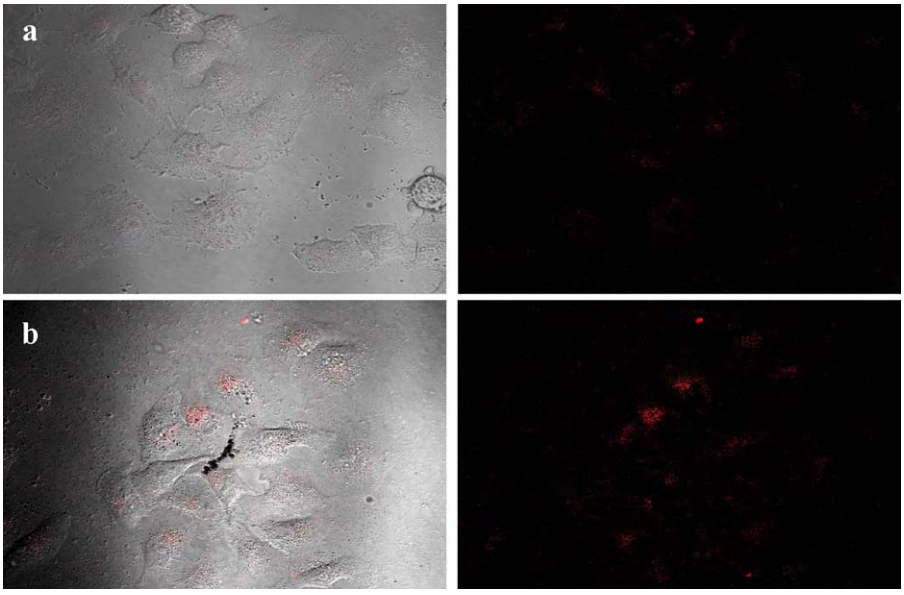


**Fig. 8.** Confocal fluorescent images of HeLa cells (left: bright-field; right: dark-field); (a) absence and (b) presence of the $Fe_3O_4$@$SiO_2$@Eu(DBM)$_3$·$2H_2O$/$SiO_2$.

the solution became clear and transparent. After removal of the external magnet and sonication, the magnetic microspheres can be rapidly redispersed again. This simple experiment confirmed that the magnetic microspheres possess good water-dispersity and magnetic separation characteristics.

### 3.6. Cell imaging

The uptakes of the $Fe_3O_4$@$SiO_2$@Eu(DBM)$_3$·$2H_2O$/$SiO_2$ microspheres by HeLa cancer cells were studied by confocal microscopy under *in vitro* conditions. Fig. 8 shows the comparable confocal fluorescent images in the absence (a) and presence (b) of the $Fe_3O_4$@$SiO_2$@Eu(DBM)$_3$·$2H_2O$/$SiO_2$. An obvious fluorescent intensity enhancement can be seen in the cells coincubated with the microspheres (Fig. 8b), which indicates that the composites were indeed internalized by the cells. In a control group experiment, the cells slightly fluorescence red light (Fig. 8a), this phenomenon may be attributed to the presence of biomolecules or other fluorescent molecules that are usually present in biological and environmental samples. In addition, cells incubated with $Fe_3O_4$@$SiO_2$@Eu(DBM)$_3$·$2H_2O$/$SiO_2$ have gross cell morphologies similar to those of control cells. This indicates that there is no adverse cell reaction in the presence of the microspheres.

The internalized microspheres would act as two highly desired functions in biomedicine: magnetic contrast agents for magnetic resonance imaging (MRI) and fluorescent probe for fluorescence imaging. Moreover, when cell-targeting moleclules or peptides are conjugated to silica surface of the prepared microspheres, the composites will be able to recognize specific cell types or organs, which makes it suitable for biomedical imaging and diagnostic applications.

## 4. Conclusion

In summary, the $Fe_3O_4$@$SiO_2$@Eu(DBM)$_3$·$2H_2O$/$SiO_2$ bifunctional magnetic fluorescence materials with core-shell nanostructures were successfully fabricated. Advantages of the luminomagnetic microspheres mainly include: (1) They improve the poor magnetic response and reduce magnetic conglomeration through the monodisperse submicrometer $Fe_3O_4$ particulates with negligible coercivity and remanence and a larger saturation magnetization as magnetic cores; (2) They eliminate fluorescence quenching through use of the $SiO_2$ isolation layer between $Fe_3O_4$ particulates and the europium fluorescent complex; (3) They enhances the fluorescent signal and increases the photostability by encapsulating the hydrophobic europium complex into hydrophilic silica shell by means of surfactant CTAB; (4) They can be uptaken by HeLa cells without adverse cell reaction and thus possess the promising applications in bioimaging and medical diagnosis.

## Acknowledgements

We gratefully acknowledge the support from the Natural Science Foundation of China (NSFC) (No. 20871083), the Department of Education of Jilin Province of China (No. 2008-371) and the Innovative Plan Foundation of Changchun Institute of Application Chemistry, CAS, China (No. CX07QZJC-29).

## References

[1] S.A. Corr, Y.P. Rakovich, Y.K. Gun'ko, Nanoscale Res. Lett. 3 (2008) 87.
[2] J. Kim, Y. Piao, T. Hyeon, Chem. Soc. Rev. 2 (2009) 372.
[3] W.J.M. Mulder, A.W. Griffioen, G.J. Strijker, D.P. Cormode, K. Niolay, Z.A. Fayad, Nanomedicine 2 (2007) 307.
[4] X. Gao, L. Yang, J.A. Petros, F.F. Marshall, J.W. Simons, S. Nie, Curr. Opin. Biotechnol. 16 (2005) 63.
[5] T.J. Yoon, J.S. Kim, B.G. Kim, K.N. Yu, M.H. Cho, J.K. Lee, Angew. Chem. Int. Ed. 44 (2005) 1068.
[6] Y.M. Huh, Y.W. Jun, H.T. Song, S.J. Kim, J.S. Choi, J.H. Lee, S. Yoon, K.S. Kim, J.S. Shin, J.S. Suh, J. Cheon, J. Am. Chem. Soc. 127 (2005) 12387.
[7] M. Liong, J. Lu, M. Kovochich, T. Xia, S.G. Ruehm, A.E. Nel, F. Tamanoi, J.I. Zink, ACS Nano 2 (2008) 889.
[8] J. Wu, Z.Q. Ye, G.L. Wang, J.L. Yuan, Talanta 72 (2007) 1693.
[9] J. Yang, C.H. Lee, H.J. Ko, J.S. Suh, H.G. Yoon, K. Lee, Y.M. Huh, S. Haam, Angew. Chem. Int. Ed. 46 (2007) 1.
[10] J. Yang, C.H. Lee, J. Park, S. Seo, E.K. Lim, Y.J. Song, J.S. Suh, H.G. Yoon, Y.M. Huh, S. Haam, J. Mater. Chem. 17 (2007) 2695.
[11] Y. Lalatonne, C. Paris, J.M. Serfaty, P. Weinmann, M. Lecouveya, L. Motte, Chem. Commun. 22 (2008) 2553.
[12] L. Wang, J. Lei, J. Zhang, Chem. Commun. 16 (2009) 2195.
[13] Y.S. Lin, S.H. Wu, Y. Hung, Y.H. Chou, C. Chang, M.L. Lin, C.P. Tsai, C.Y. Mou, Chem. Mater. 18 (2006) 5170.
[14] L. Li, E.S.G. Choo, Z.Y. Liu, J. Ding, J.M. Xue, Chem. Phy. Lett. 461 (2008) 114.
[15] K. Tao, H. Zhou, H. Dou, B. Xing, W. Li, K. Sun, J. Phys. Chem. C 113 (2009) 8762.
[16] S. Yang, H. Liu, Z. Zhang, New J. Chem. 3 (2009) 620.
[17] Y. Zhang, Sh.N. Wang, S. Ma, J.J. Guan, D. Li, X.D. Zhang, Z.D. Zhang, J. Biomed. Mater. Res. Part A 85A (2008) 840.
[18] M.J. Li, Z. Chen, V.W.W. Yam, Y. Zu, ACS Nano 2 (2008) 905.

[19] Z. Ma, D. Dosev, M. Nichkova, R.K. Dumas, S.J. Gee, B.D. Hammock, K. Liu, I.M. Kennedy, J. Magn. Magn. Mater. 321 (2009) 1368.
[20] C.W. Lai, Y.H. Wang, C.H. Lai, M.J. Yang, C.Y. Chen, P.T. Chou, C.S. Chan, Y. Chi, Y.C. Chen, J.K. Hsiao, Small 4 (2008) 218.
[21] J. Choi, J.C. Kim, Y.B. Lee, I.S. Kim, Y.K. Park, N.H. Hur, Chem. Commun. 16 (2007) 1644.
[22] D. Ma, J. Guan, F. Normandin, S. Deĭnommeĭe, G. Enright, T. Veres, B. Simard, Chem. Mater. 18 (2006) 1920.
[23] J.I. Yuan, G.L. Wang, Trends Anal. Chem. 25 (2006) 490.
[24] P.P. Xing, H.Y. Zhang, N. Li, L.L. Tong, K.H. Xu, B. Tang, Chin. J. Anal. Sci. 25 (2009) 721.
[25] N. Xiang, X.M. Zhang, L.Y. Tian, Y.Q. Bian, B.H. Zhao, Chin. J. Biol. 26 (2009) 65.
[26] Z.Y. Ma, D. Dosev, M. Nichkova, S.J. Gee, B.D. Hammock, I.M. Kennedy, J. Mater. Chem. 19 (2009) 4695.
[27] G. Wang, J. Yuan, X. Hai, K. Matsumoto, Talanta 70 (2006) 133.
[28] Z. Ye, M. Tan, G. Wang, J. Yuan, Talanta 65 (2005) 206.
[29] H.C. Lu, G.S. Yi, S.Y. Zhao, D.P. Chen, L.H. Guo, J. Cheng, J. Mater. Chem. 14 (2004) 1336.
[30] S.Y. Yu, H.J. Zhang, J.B. Yu, C. Wang, L.N. Sun, W.D. Shi, Langmuir 23 (2007) 7836.
[31] H. Deng, X.L. Li, Q. Peng, X. Wang, J.P. Chen, Y.D. Li, Angew. Chem. Int. Ed. 44 (2005) 2782.
[32] F. Bertorelle, C. Wilhelm, J. Roger, F. Gazeau, C. Menager, V. Cabuil, Langmuir 22 (2006) 5385.
[33] S.K. Mandal, N. Lequeux, B. Rotenberg, M. Tramier, J. Fattacciolo, J. Bibette, B. Dubertret, Langmuir 21 (2005) 4175.
[34] J.M. Perez, T. O' Loughlin, F.J. Simeone, R. Weissleder, L. Josephson, J. Am. Chem. Soc. 124 (2002) 2856.
[35] Y. Zhang, Z. Chen, J. Yang, J. Yangzhou Univ. (Natural Science Edition) 1 (1998) 35.
[36] F.Y. Zhao, Z. Xue, Y.L. Zhao, Chem. Reagent 24 (2002) 257.
[37] W. Stöber, A. Fink, E. Bohn, J. Colloid Interface Sci. 26 (1968) 62.
[38] Y. Deng, D. Qi, C. Deng, X. Zhang, D. Zhao, J. Am. Chem. Soc. 130 (2008) 28.